Magnetic Polarons and Large Negative Magnetoresistance in GaAs Nanowires Implanted with Mn Ions

ARTICLE *in* NANO LETTERS · OCTOBER 2013

Impact Factor: 13.59 · DOI: 10.1021/nl402229r · Source: PubMed

12 AUTHORS, INCLUDING:

Sandeep Kumar
Lund University
35 PUBLICATIONS **266** CITATIONS
SEE PROFILE

Christian Borschel
Jena
32 PUBLICATIONS **296** CITATIONS
SEE PROFILE

Anna Pertsova
Nordic Institute for Theoretical Physics
16 PUBLICATIONS **34** CITATIONS
SEE PROFILE

Carsten Ronning
Friedrich Schiller University Jena
275 PUBLICATIONS **4,535** CITATIONS
SEE PROFILE

NANO LETTERS

Letter

pubs.acs.org/NanoLett

Magnetic Polarons and Large Negative Magnetoresistance in GaAs Nanowires Implanted with Mn Ions

Sandeep Kumar,[†,■] Waldomiro Paschoal, Jr.,[†,‡,■] Andreas Johannes,[§] Daniel Jacobsson,[†] Christian Borschel,[§] Anna Pertsova,[∥] Chih-Han Wang,[⊥] Maw-Kuen Wu,[⊥,¶] Carlo M. Canali,[∥] Carsten Ronning,[§] Lars Samuelson,[†] and Håkan Pettersson[†,*,‡]

[†]Solid State Physics/The Nanometer Structure Consortium, Lund University, Box 118, SE-221 00 Lund, Sweden

[‡]Department of Mathematics, Physics and Electrical Engineering, Halmstad University, Box 823, SE-301 18, Halmstad, Sweden

[§]Institute for Solid State Physics, Friedrich-Schiller-University Jena, Max-Wien-Platz 1, D-07743 Jena, Germany

[∥]Department of Physics and Electrical Engineering, Linneaus University, SE-39233 Kalmar, Sweden

[⊥]Institute of Physics, Academia Sinica, Taipei, Taiwan

[¶]Department of Physics, National Donghwa University, Taiwan

ABSTRACT: We report on low-temperature magnetotransport and SQUID measurements on heavily doped Mn-implanted GaAs nanowires. SQUID data recorded at low magnetic fields exhibit clear signs of the onset of a spin-glass phase with a transition temperature of about 16 K. Magnetotransport experiments reveal a corresponding peak in resistance at 16 K and a large negative magnetoresistance, reaching 40% at 1.6 K and 8 T. The negative magnetoresistance decreases at elevated temperatures and vanishes at about 100 K. We interpret our transport data in terms of spin-dependent hopping in a complex magnetic nanowire landscape of magnetic polarons, separated by intermediate regions of Mn impurity spins, forming a paramagnetic/spin-glass phase.

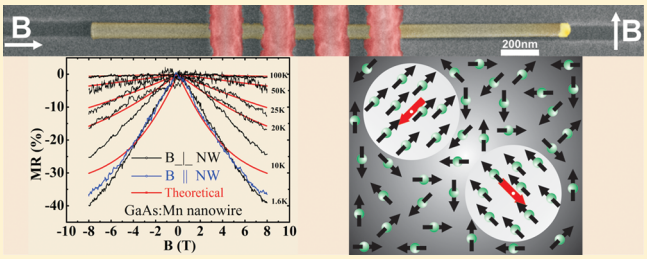

KEYWORDS: *Nanowires, ion-implantation, (Ga,Mn)As, spintronics, magnetic polarons, spin-glass, hopping transport, negative magnetoresistance*

The long-sought goal to engineer magnetic semiconductor systems on the nanometer scale poses challenges to understand magnetic properties and transport mechanisms in great detail at a fundamental level. Despite extensive studies, there is still a debate on the nature of ferromagnetic states in dilute magnetic III−V materials. Common models for (Ga,Mn)As alloys involve hole-mediated coupling of local magnetic Mn moments forming a ferromagnetic phase below a critical Curie temperature (T_C). The true nature of the states where holes provided by substitutional Mn reside, however, still remains controversial. Substitutional Mn has been proposed to strongly hybridize with the valence band states of GaAs,[1−3] or to form an impurity band[4−8] leading to the observed ferromagnetism through different exchange interactions.

Most theoretical and experimental studies so far have focused on dilute alloys with a sufficiently high concentration of Mn to achieve a high T_C.[1−8] More recently, there has been an increasing interest in semi-insulating semiconductor materials doped with magnetic elements.[9,10] Kaminski and Das Sarma[11] have proposed a magnetic polaron percolation model to explain the magnetotransport properties of dilute magnetic semiconductors (DMS) exhibiting a strong insulating character. This model assumes a heavily compensated material with both strongly localized charge carriers and a random spatial distribution of magnetic impurities. The strong exchange interaction between localized holes and magnetic impurities leads to the formation of bound spin-polarized magnetic polarons (BMPs). Yuldashev et al.[9] used this polaron model to estimate the critical concentration of holes required to form a ferromagnetic phase in (Ga,Mn)As thin films codoped with Te donors. It was demonstrated that an increased Te concentration (compensation) gradually reduces T_C, eventually replacing the long-range ordered ferromagnetic state with a paramagnetic-to spin-glass phase.

Dilute magnetic III−V nanowires (NWs) are fundamentally interesting not only for the expected new physics connected to their quasi-1D character but also because they can be monolithically integrated with silicon due to their small footprint.[12] Realizing (Ga,Mn)As NWs is thus an important step toward integration of spintronics with silicon in line with the "More than Moore" concept. ("More than Moore" implies new functionality added to conventional main-stream digital electronics beyond merely an increase in transistor density.)

Received: June 18, 2013
Revised: September 22, 2013

   dx.doi.org/10.1021/nl402229r | *Nano Lett.* XXXX, XXX, XXX−XXX

Because of low solubility of Mn in GaAs, it turns out to be extremely difficult to grow high-quality (Ga,Mn)As NWs with standard gas phase or molecular beam epitaxial techniques. Butschkow et al.[13] have studied the magnetotransport properties of core/shell NWs, which exhibit a different geometry than ours in that a thin ferromagnetic (Ga,Mn)As shell is grown around a nonmagnetic GaAs core at low temperature. These NWs exhibit a strong uniaxial anisotropy and a very pronounced negative magnetoresistance. The core/shell approach is an interesting way to circumvent the problem of growing (Ga,Mn)As NWs. Recently, we have reported on a different way to circumvent the growth problems by implanting the NWs with Mn ions after growth.[14] In this Letter, we report on magnetic properties and transport mechanisms in single-crystalline Mn-implanted GaAs NWs. Using electron beam lithography, we have fabricated contacts to individual nanowires facilitating well-controlled transport experiments. Combined with SQUID measurements on large ensembles of NWs, we present data consistent with spin-glass/paramagnetic nanowires involving bound magnetic polarons separated by intermediate unpolarized regions of Mn impurity spins.

The growth of NWs and subsequent Mn implantation were described previously.[15] Here, we summarize some key features along with improvements compared to our first implantation process described in ref 14. Single crystalline epitaxial GaAs NWs with 80 nm diameter and about 2 μm length were grown by MOVPE using monodisperse Au particles as catalysts. The NWs were grown on GaAs ⟨111⟩ substrates leading to perpendicular growth direction relative to the substrate. The NWs were implanted under an angle of 45° in respect to the nanowire axis with 100 keV Mn ions using a general purpose implanter (High Voltage Engineering Europa). The sample temperature was kept at 300 °C to facilitate efficient dynamic annealing during implantation. Using a Mn fluency of 1.8×10^{16} ions/cm^2 resulted in a total Mn concentration of about 2.5 atom % (corresponding to a stoichiometry of $(Ga_{1-x}, Mn_x)As$ with $x = 0.05$), confirmed by TEM/EDX. Figure 1 shows a two-

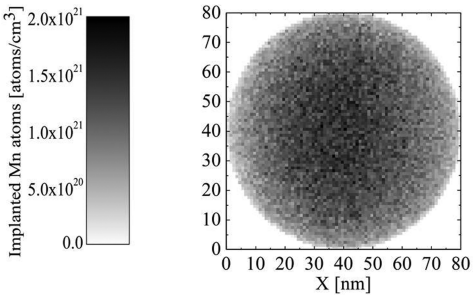

Figure 1. Cross-sectional plot of the simulated Mn distribution in a 80 nm NW implanted with 100 keV Mn^+ at an angle of 45° relative to the NW. The grayscale corresponds to a fluency of 1.8×10^{16} ions/cm^2, or a mean Mn concentration of 2.5%.

dimensional (2D) plot of the predicted implanted Mn distribution in the NWs, numerically calculated using our own developed Monte Carlo "iradina" software.[16] From this modeling, we conclude that the distribution of Mn atoms in the NWs is expected to be fairly uniform using the implantation parameters described above. For transport measurements, NWs were mechanically transferred onto a silicon substrate covered by a 210 nm thick silicon dioxide layer on which reference markers and macroscopic metal pads were predefined. Prior to transferring of the NWs, trenches were etched in the SiO_2 layer to align the wires for magnetotransport studies. Electron beam lithography was used to define contacts connecting individual NWs to the macroscopic contact pads. The samples were treated in a HCl/H_2O solution for 15 s followed by a 2 min surface passivation in a heated (40 °C) NH_4S_x/H_2O solution. Low resistivity 4-point ohmic contacts to the nanowires were made by evaporation of Pd (10 nm)/Zn (10 nm)/Pd (35 nm) after passivation. The sample processing was finalized by a lift-off process. The magnetotransport measurements were performed in a Janis VariTemp superconducting cryomagnet system (Model 8T-SVM), with the magnetic field applied in the plane of the substrate (parallel or perpendicular to the NW as defined in the inset of Figure 2). For SQUID measurements,

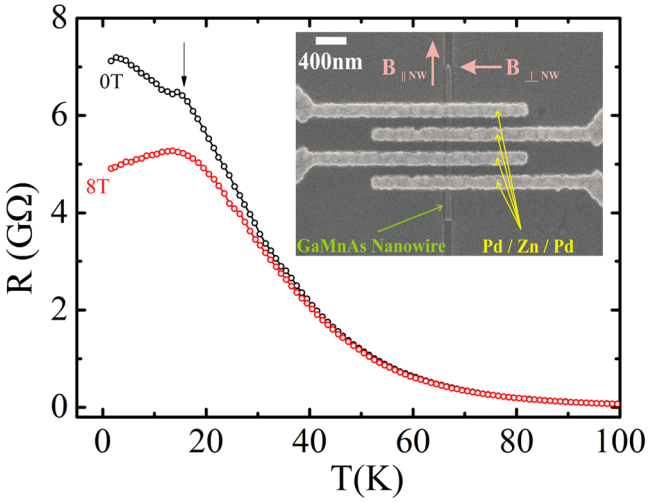

Figure 2. Magnetoresistance trace for a $(Ga_{1-x},Mn_x)As$ NW with x = 5% at 0 and 8 T, respectively. Arrow at 0 T trace indicates a transition from a high-temperature paramagnetic to low-temperature spin-glass phase. The local maximum observed in the 8 T trace possibly signals the onset of a weak ferromagnetic phase (see discussion in text). Inset shows an SEM micrograph of a NW with four electrodes for magnetotransport measurements.

large ensembles of NWs (~5×10^5) were mechanically transferred to a Si/SiO_2 substrate. The magnetic properties were measured using a SQUID-VSM magnetometer manufactured by Quantum Design Corporation. The combination of SQUID and VSM technology provides superior sensitivity (standard deviation 10^{-8} emu) and fast measurement cycles. The magnetic field applied in the SQUID experiments was applied perpendicular to the substrate surface with randomly deposited NWs.

Recently we have shown that Mn-implanted GaAs NWs are highly resistive even at room temperature.[15] The carriers (holes) are highly localized and Mott variable range hopping is the dominant transport mechanism at low temperatures. Figure 2 shows the temperature dependence of the resistance of a typical single NW. From the high resistance, it is evident that the hopping mechanism, associated with the overlap of wave function tails, indeed corresponds to a very low effective mobility. From the figure it is also evident that the resistance displays a small kink or shoulder at T_C ~16 K. A careful analysis of the curve shows that this feature is in fact a local maximum that was not observed in our previous studies,[14] most likely due to the use of thicker nanowires with less surface depletion in the present study. When a magnetic field of 8 T is applied, the

dx.doi.org/10.1021/nl402229r | Nano Lett. XXXX, XXX, XXX−XXX

resistance at $T < 100$ K is typically smaller than the zero-field resistance. Interestingly, the resistance now exhibits a clear local maximum at the same temperature (T_C). The presence of a local maximum in the resistivity versus temperature in ferromagnetic metals and semiconductors is usually an indication of critical behavior and the temperature at which it occurs is identified with the Curie temperature. Its physical origin is scattering of carriers by spin fluctuations developing at the ferromagnetic transition. In the present case, this interpretation has to be confirmed with great care since our system is far from the metallic regime. The crucial quantity determining the transport properties of the sample is the effective hole concentration. A precise determination of this quantity is challenging, primarily due to uncertainties related to possible influence of surface depletion (leading to an effective channel width smaller than the NW diameter) and to unknown hole mobility. Estimates based on resistance measurements at room temperature,[15] as well as on thermoelectric measurements,[17] indicate that the effective hole concentration is less than 10^{18} cm^{-3}. This value is much smaller than the nominal Mn impurity concentration, estimated to be $\sim 10^{21}$ cm^{-3} for a 5% Mn-doped NW. The strong reduction of the hole concentration is most likely the result of compensation by remaining postimplantation point defects, such as Mn interstitials and As antisites.

The physical picture emerging from these considerations is the one of a system composed of relatively few quasi-localized holes, each surrounded by a large number of Mn impurities. In this regime, the possible onset of a ferromagnetic transition can be analyzed by means of a theoretical model of magnetic polarons, proposed by Kaminski et al.[11] According to this model, the exchange interaction between carriers (holes) and magnetic impurities leads to the formation of BMPs, consisting of individual localized holes surrounded by magnetic impurities, whose magnetic moment is antiferromagnetically coupled to the hole magnetic moment. The effective radius of a BMP is given by[11]

$$r_{\mathrm{pol}}(T) = \frac{a_{\mathrm{B}}}{2} \ln \frac{sS|J_0|}{k_{\mathrm{B}}T} \qquad (1)$$

where a_B is the Bohr radius of the hole, J_0 is the exchange energy between the magnetic ion and the localized hole, and T is the temperature. S and s are the absolute values of the impurity spin and hole respectively. Impurity spins that are not found inside a sphere of radius r_{pol}, centered at a localized hole, are essentially free. The radius of the BMP increases with decreasing temperature. When BMPs start to overlap, larger regions with the same magnetization orientation appear and eventually long-range ferromagnetic order can be established in the system via a percolation phase transition. The transition temperature will increase with the hole concentration n_h. More precisely, for a given value of n_h the condition for a magnetic percolation transition is given by

$$r_{\mathrm{pol}}(n_{\mathrm{h}})^{1/3} \approx 0.86 \qquad (2)$$

which expresses the simple fact that the average distance between two localized holes is approximately equal to the polaron radius. The critical temperature can be estimated from eq 1. In Figure 3, we plot the polaron radius as a function of temperature using eq 1 with $J_0 = 15$ meV, and $a_B = 1.39$ nm.[9] We can see that the polaron radius remains much smaller than the NW radius even at very low temperatures, justifying the use

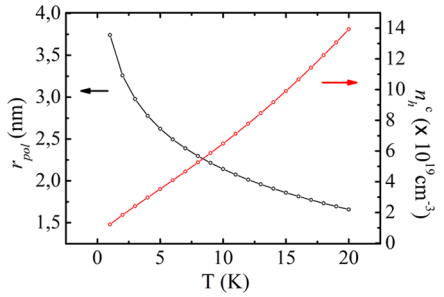

Figure 3. Black curve shows the theoretical estimate of the polaron radius obtained from eq 1. Red curve shows the critical hole density versus temperature, defined as the density satisfying the magnetic percolation transition condition given in eq 2 at a given temperature.

of the model by Kaminski et al. also for our quasi-1D systems. Figure 3 also shows the critical hole density, n_h^c, versus temperature that is the hole density satisfying eq 2 for a given temperature. This plot indicates quite definitely that the hole density required to trigger a magnetic percolation transition in the absence of an external magnetic field is much larger than the estimated hole density of the NWs for all accessible temperatures. In particular, the kink in the resistance observed at ~16 K can hardly be associated with a ferromagnetic transition. This conclusion is further supported by temperature-dependent zero-field-cooled (ZFC) and field-cooled (FC) magnetization measurements on large ensembles of NWs. Temperature-dependent ZFC and FC magnetization curves recorded at 3 mT are shown in Figure 4. In the temperature

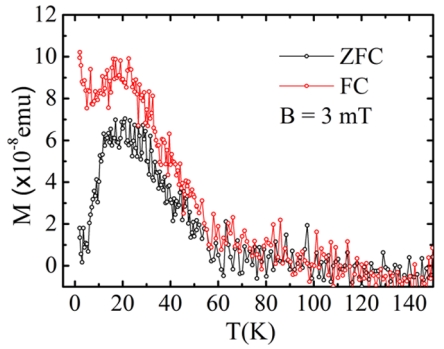

Figure 4. Temperature-dependent ZFC and FC magnetization curves of Mn implanted GaAs nanowire ensembles at an applied magnetic field of 3mT applied perpendicular to the substrate surface with deposited NWs.

range 20 K < T < 100 K, the magnetization is the same for both cases and it increases with decreasing temperature. Interestingly, the two curves start to diverge below 20 K and while the ZFC magnetization goes rapidly to zero the FC does not and in fact shows a hint of further increasing with decreasing temperature. Note that the peak in the ZFC curve occurs in the vicinity of the critical temperature where the resistance in Figure 2 exhibits a kink. We have also made the observation that the peak temperature (so-called blocking temperature) in ZFC curves decreases with increasing magnetic field strength. The divergence of FC and ZFC curves is less pronounced at increasing field strength, and completely vanishes at applied fields >20 mT.

This behavior is typically associated with a phase transition from a paramagnetic state to a spin-disordered or spin-glass

dx.doi.org/10.1021/nl402229r | Nano Lett. XXXX, XXX, XXX−XXX

state in DMSs,[18] and it has been observed previously in semi-insulating $Ga_{1-x}Mn_xAs$ thin films.[9] In order to interpret this phenomenon, the BMP model must be somewhat modified[19] to the case of a very low hole concentration where the average distance between two localized holes, that is, distance between centers of two distinct adjacent polarons, is large. Clearly the radius of a BMP, containing magnetic impurities all aligned along the opposite direction of the hole spin, cannot increase indefinitely by decreasing T. Beyond a certain size L, the long-range exchange coupling between the hole spin and impurity spins far away from the polaron center becomes comparable to the relatively weaker direct exchange interaction between nearby impurities, which is typically antiferromagnetic. The interplay between these two competing interactions in the intermediate regions between magnetic polarons prevents the onset of long-range order and can result in a spin-disordered ground state. In this scenario, well-defined BMPs are still present, but they are separated by large intermediate unpolarized regions where the impurity spins at low-temperature freeze into a spin-glass-like state. Following ref 19, we can analyze the competition between the ferromagnetic and the spin-glass phase by introducing a parameter $P = (n_h^{1/3}a_B)/(n_i^{1/3}l)$, where l is the decay length of the antiferromagnetic interaction between magnetic impurities and n_i is the doping concentration. If $P \gg 1$, long-range ferromagnetic order is established via the magnetic percolation transition. On the other hand if $P \ll 1$, although magnetic polarons still form their interaction with the frustrated medium of magnetic impurity moments in the intermediate region leads to a spin-glass ground state. Using the estimates for the hole and impurity concentrations for the present NWs mentioned above, and further assuming l to be of the order of the impurity radius ~0.1 nm[19,20] and $a_B \sim 1.39$ nm, yields $P \leq 1$. These considerations support the picture of a ground state characterized by a spin-disordered phase. Note that in the presence of a strong magnetic field, the situation is different. This is already obvious from Figure 2, where the clear local maximum in resistance at 8 T indicates that the system is most likely in a phase close to ferromagnetic.

In the last part, we discuss magnetoresistance measurements and propose a phenomenological model that captures the experimental behavior remarkably well in the relevant temperature regime. The black and blue traces in Figure 5 show the temperature dependence of the magnetoresistance (MR) defined as $MR(\%) = [R(B,T) - R(0,T)]/[R(0,T)]$, where $R(B,T)$ is the resistance at magnetic field strength B and temperature T. Evidently, there is a remarkably large negative MR reaching 40% at 8 T with no hysteresis i.e. $R(B) = R(-B)$. We have studied six NW devices in great detail and they all display the same characteristic transport properties with a MR ratio between 40 and 50% and a kink/local resistance maximum at T_C ~16 K. MR data for magnetic fields applied perpendicular and parallel to a NW, respectively, display no significant differences as shown in Figure 5. The basic features of the negative MR curves plotted in Figure 5 can be understood in the context of the BMP model, which was used successfully in the first part of the paper to explain the observed transition to a spin disordered phase at low temperatures. Here, however, the magnetic polaron picture is adjusted to account for the presence of magnetic field and elevated temperatures. On the one hand, the BMP model suggests that as the applied magnetic field is increased, the magnetic moments of polarons successively become aligned with the field. This would facilitate an enhanced spin-dependent hopping between adjacent polarons, leading to a decrease of the resistance and hence to an increased MR as defined above. On the other hand, increasing the magnetic field also leads to an increased ordering of the random spin texture in the unpolarized region, which also enhances hopping from a polaron to a partially ordered intermediate site. Interestingly, the observed MR in our NWs is about 10 times larger than typically observed in metallic (Ga, Mn)As thin films,[21,22] pointing to strong spin-dependent scattering mechanisms involved in hopping transport in comparison to valence band transport. However, it is not obvious which of the possible mechanisms, for example, spin-dependent hopping between polarons whose magnetic moments align with field or hopping through partially ordered intermediate regions of Mn spins, provides the dominant contribution to the MR. Furthermore, both mechanisms are relevant for understanding the temperature dependence of the MR. Increasing the temperature causes progressive randomization of the orientation of magnetic polaron moments, in turn leading to a decreased MR. However, as the temperature is increased, the BMP radius decreases (see Figure 3) and therefore the intermediate regions between polarons become larger. Estimating the average number of Mn ions within the polaron volume shows that at temperatures above 16 K a typical polaron contains only a few Mn ions with the majority of impurity spins being in the intermediate region ($N_{Mn} \leq 4$ for $r_{pol} \approx 1$ nm taken as an average of the expression in eq 1 in the range 16 K < T < 100 K). The polaron radius is thus considerably smaller than the average separation between two polarons. This suggests that at elevated temperatures the paramagnetic behavior of Mn spins in the intermediate regions cannot be ignored.

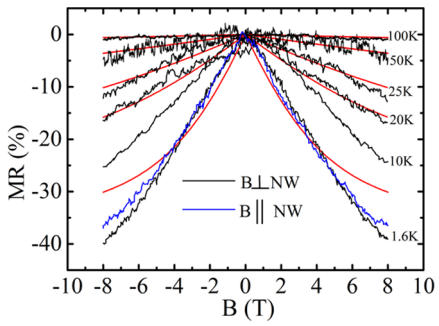

Figure 5. Magnetoresistance (black) traces recorded for a (Ga_{1-x}, Mn_x)As NW with x = 5% with magnetic fields applied perpendicular to the NW (see inset of Figure 2 for definition of field directions). Red traces are theoretical MR curves calculated from eq 7 (10−100K). The blue trace shows the corresponding temperature dependence of the magnetoresistance with the magnetic field applied parallel to the NW (1.6 K).

We now propose a phenomenological model, incorporating the ideas above, which is able to capture the decrease of the resistance at finite magnetic fields and in addition provides insight into which mechanism is most likely responsible for the large negative MR. In the presence of magnetic field, the hopping of a hole is assumed to have an activation form

$$R \propto \exp\left(\frac{\Delta E}{k_B T}\right) \quad (3)$$

dx.doi.org/10.1021/nl402229r | Nano Lett. XXXX, XXX, XXX−XXX

where ΔE is the change of the hopping energy with magnetic field. We further postulate that ΔE is proportional to the interaction energy between the spin of the hole s and an average spin $\langle S_i \rangle$ of a magnetic object, which can represent a magnetic polaron or Mn ion in the unpolarized region. Since both mechanisms are relevant, we leave S, the spin angular momentum of the magnetic object, as a variable parameter in our model. Although the value of the interaction energy is also not known, we take it proportional to the only energy scale in our problem that is the exchange interaction between the hole and the magnetic object. To account for the presence of BMPs, we assume that the hopping distance might still be regulated by the effective hole (and indeed polaron) separation, and therefore ΔE will be proportional to n_h. The hopping event is also likely to be proportional to the typical interaction range of the hole wave function a_B. Finally, the average spin of the magnetic object in the presence of a magnetic field is given by

$$\langle S_i \rangle = S\mathcal{B}_S\left(\frac{Sg\mu_B B}{k_B T}\right) \tag{4}$$

where $\mathcal{B}_S\left(\frac{Sg\mu_B B}{k_B T}\right)$ is the Brillouin function and defined as[23]

$$\mathcal{B}_S\left(\frac{Sg\mu_B B}{k_B T}\right) = \frac{2S+1}{2S}\coth\left[\frac{2S+1}{2S}\left(\frac{Sg\mu_B B}{k_B T}\right)\right] - \frac{1}{2S}\coth\left[\frac{1}{2S}\left(\frac{Sg\mu_B B}{k_B T}\right)\right] \tag{5}$$

where S is the effective spin, $g = 2$ is the gyromagnetic ratio and μ_B is the Bohr magneton.

A possible form of ΔE is therefore

$$\Delta E = -A\frac{4\pi}{3}a_B^3 n_h J_0 s S\mathcal{B}_S\left(\frac{Sg\mu_B B}{k_B T}\right) \tag{6}$$

where A is constant. The resulting magnetic field dependence of the resistance is given by

$$R(B, T) = R(0, T)\exp\left(-\frac{A4\pi a_B^3 n_h J_0 s S}{3k_B T}\mathcal{B}_S\left(\frac{Sg\mu_B B}{k_B T}\right)\right) \tag{7}$$

In Figure 6 we show the result of fitting eq 7 to the measured resistance data for different values of the magnetic field. Interestingly, the best fitting for all relevant values of the magnetic field is obtained for $S = 5/2$ (spin of single Mn impurity) and $A \sim 2$. We also note that the fitting proposed here predicts that the decrease of the resistance as a function of field should saturate at $B \sim 20$ T. Furthermore, at 100 K all the MR signal has disappeared even in the presence of a magnetic field of 8 T. The fitting performs remarkably well in the temperature range roughly between 20 and 100 K but fails to predict the MR below 20 K where a glitch in the experimental data signals the aforementioned phase transition. Figure 6 suggests that above the spin-glass transition temperature, $R(B,T)$, can be described mainly by a paramagnetic state of magnetic impurities in the intermediate regions between BMPs, while below the transition temperature the system enters into a spin-glass state. In the presence of a strong magnetic field, the transition to a spin-glass state is transformed into a transition to a state that is most likely close to being ferromagnetic. This is brought about by the alignment of the impurity spins in the intermediate regions, as well as the magnetic moments of the polarons. Equation 7 can also be used to calculate the expected MR ratio versus magnetic field. In Figure 5, we include these MR curves at the corresponding temperatures. Evidently, there is a good agreement between experiment and theory for temperatures above 20 K. At lower temperatures, there is a significant deviation related to the phase transition discussed above.

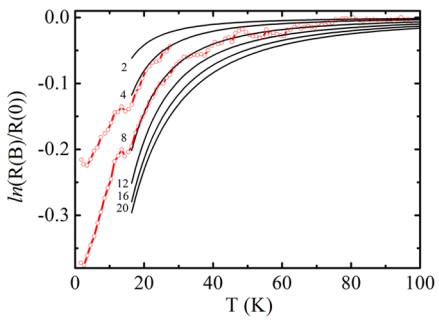

Figure 6. Red traces show experimental magnetoresistance ratios at 4 and 8T, respectively. Black lines are corresponding theoretical curves at different magnetic fields from 2 to 20T, calculated from eq 7.

In conclusion, we have performed magnetotransport measurements on single (Ga, Mn)As NWs. At $T < 100$ K, a large negative magnetoresistance associated with spin-dependent hopping transport is observed. In the absence of external field a spin-glass phase is formed below $T_C \sim 16$ K, as a result of the competition between the long-range hole-Mn and short-range Mn−Mn exchange interactions. When a strong magnetic field is present, the system below T_C is rather described by a phase close to being ferromagnetic. We interpret our transport data in terms of strongly spin-dependent hopping mechanisms involving magnetic polarons and large partially ordered intermediate regions of Mn impurity spins, forming a paramagnetic/spin-glass phase. Mn-implanted NWs represent an interesting novel type of nanometer-scale building blocks for miniaturized spintronic devices compatible with main-stream silicon technology.

AUTHOR INFORMATION

Corresponding Author

*E-mail: hakan.pettersson@hh.se.

Author Contributions

■S.K. and W.P. contributed equally to this work and are cofirst authors.

Notes

The authors declare no competing financial interest.

ACKNOWLEDGMENTS

The authors thank Magnus Borgström and Jesper Wallentin for help with providing GaAs nanowires and Maria Messing for TEM/EDX studies. Furthermore, the authors acknowledge financial support from nmC@LU, the Swedish Research Council (VR), the Knut and Alice Wallenberg Foundation, the Swedish National Board for Industrial, Technological Development, the Swedish Foundation for Strategic Research, the Nordforsk research network "Nanospintronics; theory and simulations", and the German Research Society (DFG) project Ro1198/14. One of the authors, W. P, gratefully acknowledges financial support from the Pará Education Secretary (SEDUC) and the Pará Government School (EGPA).

REFERENCES

(1) Dietl, T.; Ohno, H.; Matsukura, F.; Cibert, J.; Ferrand, D. *Science* **2000**, *287*, 1019.
(2) Neumaier, D.; Turek, M.; Wurstbauer, U.; Vogl, A.; Utz, M.; Wegscheider, W.; Weiss, D. *Phys. Rev. Lett.* **2009**, *103*, 087203.
(3) Masek, J.; Maca, F.; Kudrnovsky, J.; Makarovsky, O.; Eaves, L.; Campion, R. P.; Edmonds, K. W.; Rushforth, A. W.; Foxon, C. T.; Gallagher, B. L.; Novak, V.; Sinova, J.; Jungwirth, T. *Phys. Rev. Lett.* **2010**, *105*, 227202.
(4) Burch, K. S.; Shrekenhamer, D. B.; Singley, E. J.; Stephens, J.; Sheu, B. L.; Kawakami, R. K.; Schiffer, P.; Samarth, N.; Awschalom, D. D.; Basov, D. N. *Phys. Rev. Lett.* **2006**, *97*, 087208.
(5) Ando, K.; Saito, H.; Agarwal, K. C.; Debnath, M. C.; Zayets, V. *Phys. Rev. Lett.* **2008**, *100*, 067204.
(6) Dobrowolska, M.; Tivakornsasithorn, K.; Liu, X.; Furdyna, J. K.; Berciu, M.; Yu, K. M.; Walukiewicz, W. *Nat. Mater.* **2012**, *11*, 444.
(7) Rokhinson, L. P.; Lyanda-Geller, Y.; Ge, Z.; Shen, S.; Liu, X.; Dobrowolska, M.; Furdyna, J. K. *Phys. Rev. B* **2007**, *76*, 161201.
(8) Ohya, S.; Takata, K.; Tanaka, M. *Nat. Phys.* **2011**, *7*, 342.
(9) Yuldashev, Sh. U.; Jeon, H. C.; Im, H. S.; Kang, T. W.; Lee, S. H.; Furdyna, J. K. *Phys. Rev. B* **2004**, *70*, 193203.
(10) Sheu, B. L.; Myers, R. C.; Tang, J.-M.; Samarth, N.; Awschalom, D. D.; Schiffer, P.; Flatte, M. E. *Phys. Rev. Lett.* **2007**, *99*, 227205.
(11) Kaminski, A.; Das Sarma, S. *Phys. Rev. Lett.* **2002**, *88*, 247204.
(12) Krogstrup, P.; Popovitz-Biro, R.; Johnson, E.; Madsen, M. H.; Nygard, J.; Shtrikman, H. *Nano Lett.* **2010**, *10*, 4475.
(13) Butschkow, C.; Reiger, E.; Rudolph, A.; Geißler, S.; Neumaier, D.; Soda, M.; Schuh, D.; Woltersdorf, G.; Wegscheider, W.; Weiss, D. *Phys. Rev. B* **2013**, *87*, 245303.
(14) Borschel, C.; Messing, M. E.; Borgström, M. T.; Paschoal, W., Jr.; Wallentin, J.; Kumar, S.; Mergenthaler, K.; Deppert, K.; Canali, C. M.; Pettersson, H.; Samuelson, L.; Ronning, C. *Nano Lett.* **2011**, *11*, 3935.
(15) Paschoal, W., Jr.; Kumar, S.; Borschel, C.; Wu, P.; Canali, C. M.; Ronning, C.; Samuelson, L.; Pettersson, H. *Nano Lett.* **2012**, *12*, 4838.
(16) Borschel, C.; Ronning, C. *Nucl. Instrum. Methods, Sect. B* **2011**, *269*, 2133.
(17) Wu, P.; Paschoal, W., Jr.; Kumar, S.; Borschel, C.; Ronning, C.; Canali, C. M.; Samuelson, L.; Pettersson, H.; Linke, H. *J. Nanotechnol.* **2012**, *2012*, 480813.
(18) Oseroff, S.; Keesom, P. H. *Dilute Magnetic Semiconductors*; Academic: New York, 1988; p 73.
(19) Kaminski, A.; Galitski, V. M.; Das Sarma, S. *Phys. Rev. B* **2004**, *70*, 115216.
(20) Jungwirth, T.; Gallagher, B. L.; Wunderlich, J. In *Spintronics*; Dietl, T., Awschalom, D. D., Kaminska, M., Ohno, H., Eds.; Elsevier: Amsterdam, 2008.
(21) Matsukura, F.; Ohno, H.; Shen, A.; Sugawara, Y. *Phys. Rev. B* **1998**, *57*, R2037.
(22) Omiya, T.; Matsukura, F.; Dietl, T.; Ohno, Y.; Sakon, T.; Motokawa, M.; Ohno, H. *Phys. E* **2000**, *7*, 976.
(23) Kittel, C. *Introduction to Solid State Physics*, 8th ed.; Wiley: New York, 2004.

dx.doi.org/10.1021/nl402229r | *Nano Lett.* XXXX, XXX, XXX−XXX